Optical Engineering

OpticalEngineering.SPIEDigitalLibrary.org

Starting point designs for freeform four-mirror systems

Jonathan C. Papa
Joseph M. Howard
Jannick P. Rolland

SPIE.

Jonathan C. Papa, Joseph M. Howard, Jannick P. Rolland, "Starting point designs for freeform four-mirror systems," *Opt. Eng.* **57**(10), 101705 (2018), doi: 10.1117/1.OE.57.10.101705.

Starting point designs for freeform four-mirror systems

Jonathan C. Papa,[a,*] Joseph M. Howard,[b] and Jannick P. Rolland[a]
[a]University of Rochester, Institute of Optics, Rochester, New York, United States
[b]NASA Goddard Space Flight Center, Greenbelt, Maryland, United States

Abstract. Driven by the development of freeform four-mirror solutions, we review and compare analytical methods to generate starting point designs with various states of correction, surface types, symmetry, and obscuration. The advantages and disadvantages of each are examined. We have combined several concepts and techniques from the literature to analytically generate unobscured freeform starting point designs that are corrected through the third-order image degrading aberrations. The surfaces in these starting point designs are described as base off-axis conics that image stigmatically for the central field point, also known as Cartesian reflectors, with an aspheric departure "cap" (quartic with the aperture) added to the Cartesian reflectors. Tilt angles are chosen to cancel field-asymmetric field-linear astigmatism and unobscure the system. Paraxial data from an equivalent on-axis system are used to solve a system of linear equations to determine the magnitude of the aspheric departure "caps" that are placed on top of the base Cartesian reflectors, in order to eliminate the remaining third-order image degrading aberrations. In this approach, each aspheric departure "cap" is centered about the intersection of the optical-axis-ray, also known as the base ray, with the base surface, rather than being centered about the axis of rotational invariance. [DOI: 10.1117/1.OE.57.10.101705]

Keywords: freeform; aberrations; telescopes.

Paper 171744SSP received Nov. 1, 2017; accepted for publication May 31, 2018; published online Jun. 21, 2018.

1 Introduction

Before optimizing any optical system in software, suitable starting point designs must be chosen. A suitable starting design is one that has the desired first-order properties and geometry, may be corrected for different orders of aberrations, or has a potential for aberration correction. There are several different analytical design approaches that can be used to generate a starting point design, each with their own advantages and disadvantages, which are discussed in the context of surface type, symmetry type, and aberration correction type.

Three surface types, spheres, conics, and "grown" surfaces, are considered in discussing starting points, as shown in Table 1. Starting with spherical surfaces may be desirable if the goal is to minimize the surfaces' deviation from a best-fit sphere for the purpose of manufacturability. Another advantage is that setting up a spherical starting point design in lens design software is simpler than other surface types. However, spherical surface starting points have fewer degrees of freedom for aberration correction.[1] Conic surfaces allow more degrees of freedom for aberration correction, but conic surface starting points may start off with large deviations from a best-fit sphere. However, if the goal is to minimize departure from a conic for testability with null optics, they constitute a viable path.[2,3] "Grown" surfaces are solved for using differential equations and are freeform surfaces. The freeform "grown" surfaces have more degrees of freedom for aberration compared to conic surfaces but are the most complicated to implement and are currently limited to two mirrors (a four-mirror system can be generated by putting two "grown" surface systems back-to-back).[4,5]

*Address all correspondence to: Jonathan C. Papa, E-mail: jpapa@ur.rochester.edu

The two symmetry types shown in Table 1 are rotational and plane. For obscured starting points, rotational symmetry may be considered. For unobscured starting points, rotationally symmetric systems can be made unobscured by offsetting the aperture, biasing the field, or a combination of both. The aberration theory for rotational symmetry is simpler than the aberration theory for plane symmetry. However, unobscured rotationally symmetric starting points are inconvenient to implement in lens design software if one wants to add freeform terms centered about the optical-axis-ray (OAR),[6] also known as the base ray.[7] Unobscured rotationally symmetric starting points also do not have degrees of freedom for choosing the desired folding angles and geometry. Unobscured planar-symmetric systems have more degrees of freedom to choose the folding angles and geometry, and the mirrors' vertices are conveniently centered about the base ray for these types of systems. However, the aberration theory for unobscured planar-symmetric systems is more complex.[8]

The aberration correction types shown in Table 1 are stigmatic imaging at each surface, correction through third-order, and aplanatic. Systems that satisfy stigmatic imaging at every surface not only require conic surfaces, but also the conic surfaces must operate at specific conjugates such that the individual surface contributions to spherical aberration are all zero; these types of surfaces are also referred to as Cartesian reflectors, and a system made of only Cartesian reflectors is known as a system of confocal conics. The main advantage of these types of systems is that they are corrected for all orders of spherical aberration. However, these types of systems can only be corrected through third-order if they are afocal, or if the absolute value of the magnification is 1.[9] Systems with spherical surfaces that are corrected through third-order have the advantage of better performance

Table 1 Comparison of starting point design methods with pros and cons, grouped by surface type.

Freeform surface starting point	Method	Pros	Cons
Spherical	Four tilted spherical mirrors[1]	Plane symmetry	Does not correct higher order aberrations
	Rotationally symmetric all-spherical solutions[10]	Corrected through third-order	Rotationally symmetric
Conic (including off-axis subapertures)	Rotationally symmetric all-conic solutions[9]	Stigmatic imaging at every surface, corrected through third-order	Afocal or 1× Mag only, rotationally symmetric
	Solutions from Korsch[9]	Corrected through third-order	Rotationally symmetric
	Off-axis conic layout tool	Stigmatic imaging at every surface, plane symmetry	Does not correct higher order aberrations
	Off-axis conics from aberration coefficients for plane-symmetry[8]	Stigmatic imaging at every surface, corrected through third-order, plane symmetry	Afocal or 1× Mag Only
"Grown" surfaces	Generalized sine condition for the design of aplanatic optical systems[5]	Aplanatic, plane symmetry	Two-mirror
	Afocal two freeform mirror[4]	Aplanatic, plane symmetry	Two-mirror

starting off, at the expense of degrees of freedom for the geometry of the system.[10] When evolving these various starting points to freeform solutions, the aberration theory of freeform surfaces may further reveal best starting points in the folded geometry,[11,12] with the aim to reach diffraction-limited performance across large field of views and low F-numbers.

In the remainder of this paper, we will describe in Sec. 2 how starting point methods are combined. In Sec. 3, we show an example design generated using the starting point method described in Sec. 2 to illustrate the method's efficacy.

2 Combination of Starting Point Methods

To generate starting points for freeform designs that are unobscured and corrected through the third-order image degrading aberrations, a combination of some of the methods from Table 1 is used, as discussed in Secs. 2.1–2.3. The surfaces that are generated with the procedure described here can be thought of as off-axis sections of stigmatically imaging conics with aspheric caps on top. By aspheric, we mean quartic with the radial coordinate of the part. However, these aspheric caps are centered about where the OAR intersects the surface, not about the axis of rotational symmetry for the underlying off-axis conic. The purpose of the aspheric caps is to correct for the field aberrations of field-linear coma and field-quadratic astigmatism while keeping the sum of spherical aberration zero.

2.1 *Properties of Planar-Symmetric Confocal Conic Systems*

Confocal conic systems are systems that are composed entirely of Cartesian reflectors, which are off-axis conics being used stigmatically. When the rotational symmetry of a confocal conic system is broken by tilting and decentering the mirrors to render it unobscured, it still does not have spherical aberration of any order nor any other field-constant aberrations (provided that the surface shapes are still Cartesian reflectors), because there is always a node at the center of every aberration field; additionally, systems composed of Cartesian reflectors do not have anamorphism.[8] Ignoring distortion and piston terms, the remaining third-order image degrading aberrations are field-linear coma, field-asymmetric field-linear astigmatism, field-quadratic astigmatism, and field curvature. The only aberration out of these that would not be found in a system with rotational symmetry is field-asymmetric field-linear astigmatism. An example of a system limited by field-asymmetric field-linear astigmatism is given in Sec. 3.2. If designers can eliminate the field-linear field-asymmetric astigmatism in a system of confocal conics, they can eliminate the remaining third-order aberrations using aspheric deformations about the OAR or base ray, as further explained in Sec. 2.2.

In a rotationally symmetric confocal conic system, the Cartesian reflectors are often described with the parameters R and k, where R is the radius of curvature and k is the conic constant. When breaking the rotational symmetry of a confocal conic system to yield an unobscured planar-symmetric system, three parameters are used to describe the Cartesian reflectors. These parameters can be R, k, and an offset parameter, such as decenter in the y direction. However, we use the parameters l_o, l_i, and θ, where l_o is the distance from the local coordinate system origin to the object point (i.e., central field point, which lies on the OAR), l_i is the distance from the local coordinate system origin to the image, and θ is the angle of incidence of the OAR at the local coordinate system origin of the surface. In this description of Cartesian reflectors, the sag, slope in x, and slope in y of the surface are all zero at the local coordinate system origin. This is a convenient property because the CODE V decenter type "decenter and bend" can be used, where the tilt angle of the surface "alpha" can be set to θ (i.e., the angle of incidence of the OAR at the current surface), resulting in the OAR intersecting the local coordinate system

origin of the next surface after reflecting of the current one. The sag of the freeform surfaces generated with the combination of methods proposed here constitutes a starting point to the final freeform surfaces optimization. Their sag can be decomposed into the base Cartesian reflector sag and the aspheric cap:

$$\mathrm{Sag}(x,y) = \mathrm{Sag}_{\text{Cartesian Reflector}}(l_o, l_i, \theta, x, y) + A(x^2+y^2)^2, \tag{1}$$

where $\mathrm{Sag}(x,y)$ is the total sag of the surface in the local coordinate system as a function of local coordinates x and y. $\mathrm{Sag}_{\text{Cartesian Reflector}}(l_o, l_i, \theta, x, y)$ is the sag of the Cartesian reflector as a function of object and image distances, l_o and l_i, angle of incidence of the OAR, θ, and the local coordinates x and y, whose expression is detailed in Appendix. The aspheric cap coefficient, A, specifies the magnitude of the surface term that is quartic with radial coordinate of the surface.

The first-order properties of a confocal conic system, made of a chain of Cartesian reflectors described by Eq. (1), obey the thin lens equation:

$$\Phi = -\frac{n}{f} = \frac{n'}{f'} = \frac{n'}{l_i} - \frac{n}{l_o}, \tag{2}$$

where Φ is the power of the optical surface, f is the front focal length, f' is the back focal length, n is the index of refraction before the surface, n' is the index of refraction after the surface, and l_o and $l_i$are the signed object and image distances, respectively. All local coordinate systems adopt a right-handed frame of reference. With this sign convention, a negative distance indicates that the associated z coordinate is negative in the local coordinate system. Figures 1–3 show Cartesian reflectors described by the parameters in Eq. (1), for different configurations. Respectively, they are an ellipse, a hyperbola, and a parabola. The angle θ, defined from the normal to the ray, is positive for object points that are in the quadrant of the local coordinate system, where $z < 0$ and $y > 0$ or for object points that are in the quadrant, where $z > 0$ and $y < 0$; this convention was conveniently chosen as it matches CODE V convention, which is the software we chose to interface with.

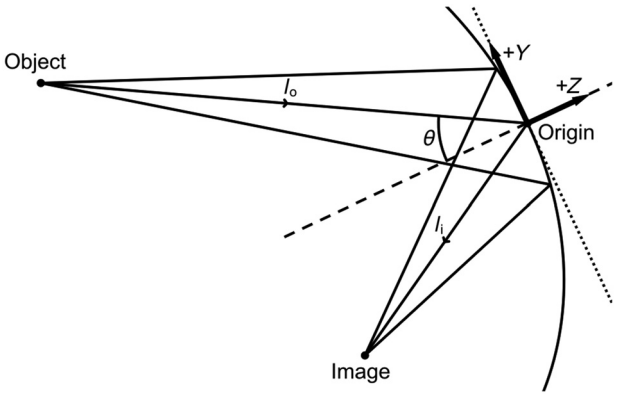

Fig. 1 Elliptical Cartesian reflector, stigmatically imaging from a real object point to a real image point. The surface is described by the three parameters, l_o, l_i, and θ, in the local coordinate system. The z axis defines the normal to the surface at the intercept of the OAR.

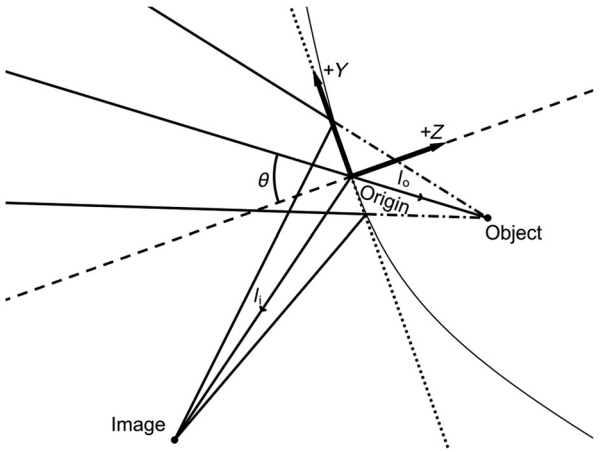

Fig. 2 Hyperbolic Cartesian reflector, stigmatically imaging from a virtual object point to a real image point. The surface is described by the three parameters, l_o, l_i, and θ, in the local coordinate system. The z axis defines the normal to the surface at the intercept of the OAR.

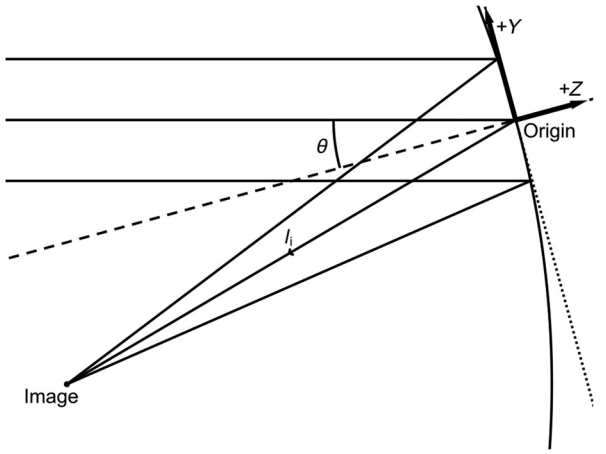

Fig. 3 Parabolic Cartesian reflector, stigmatically imaging from an object point at infinity to a real image point. The surface is described by the three parameters, l_o (at infinity), l_i, and θ, in the local coordinate system. The z axis defines the normal to the surface at the intercept of the OAR.

2.2 *Eliminating Field-Linear Field-Asymmetric Astigmatism in a Confocal Conic System*

One of the key insights from nodal aberration theory is that it is possible to find tilted/decentered systems that exhibit aberrations of the "ordinary" kind, where two astigmatism nodes collapse to a single node at the center of the field while keeping the coma node at the center of the field as well.[13,14] In Fig. 4(a), there is an astigmatism field with one node and it looks like "ordinary" field-quadratic astigmatism, whereas in Fig. 4(b), there are two nodes exemplifying binodal astigmatism. Additionally, tilted aspheric terms that are not decentered produce aberrations of the "ordinary kind," meaning field-linear coma, and field-quadratic astigmatism,[13] which is why the aspheric caps used in the proposed method need to be centered around the intersection of the OAR with the surface and not centered around the axis of rotational symmetry of the surface.

To cancel field-asymmetric field-linear astigmatism, the designer needs to select the right combination of mirror

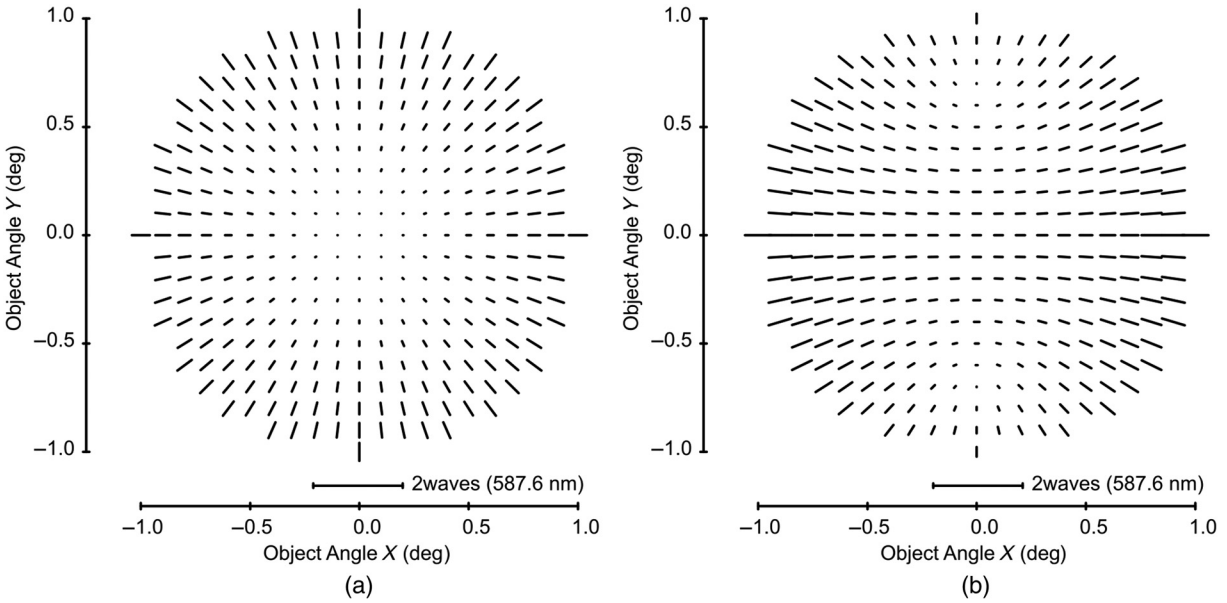

Fig. 4 Aberration plots: (a) full-field display of Z5/Z6 Fringe Zernike astigmatism showing one astigmatism node in the center ("ordinary" field-quadratic astigmatism) and (b) full-field display with two astigmatism nodes (binodal astigmatism).

tilts [i.e., θ in Eq. (1)]. Figure 5 displays an example of a two-mirror system made of confocal conics in a rotationally symmetric case and a planar-symmetric case. The primary, which is a parabola, shares one of its conic foci with the secondary, which is a hyperbola. The shared focus is marked with an X. Figure 5(a) shows the rotationally symmetric system. In Fig. 5(b), a tilted geometry is shown, and while the tilt on the primary is increased to render an unobscured system, the tilt on the secondary is solved to cancel field-asymmetric field-linear astigmatism. In this configuration, the astigmatism across the field of view has a single node in the center and is "ordinary." As the tilt on the primary increases, the tilt on the secondary must increase as well to keep linear astigmatism canceled.

There are different ways to solve for the angle on the last mirror in a confocal conic system that cancels linear astigmatism. One way is to use the aberration coefficients for planar-symmetric systems.[8] Another way is to use the closed form of the linear astigmatism free condition for a system of confocal conics.[15] In this paper, we use the latter.

2.3 *Solving for the Aspheric Caps*

Correcting the Seidel third-order aberrations in a given first-order layout for a rotationally symmetric system of four mirrors using aspheric deformations may be achieved via a linear system of equations. [16] It is important to note that a system made of Cartesian reflectors can only be corrected

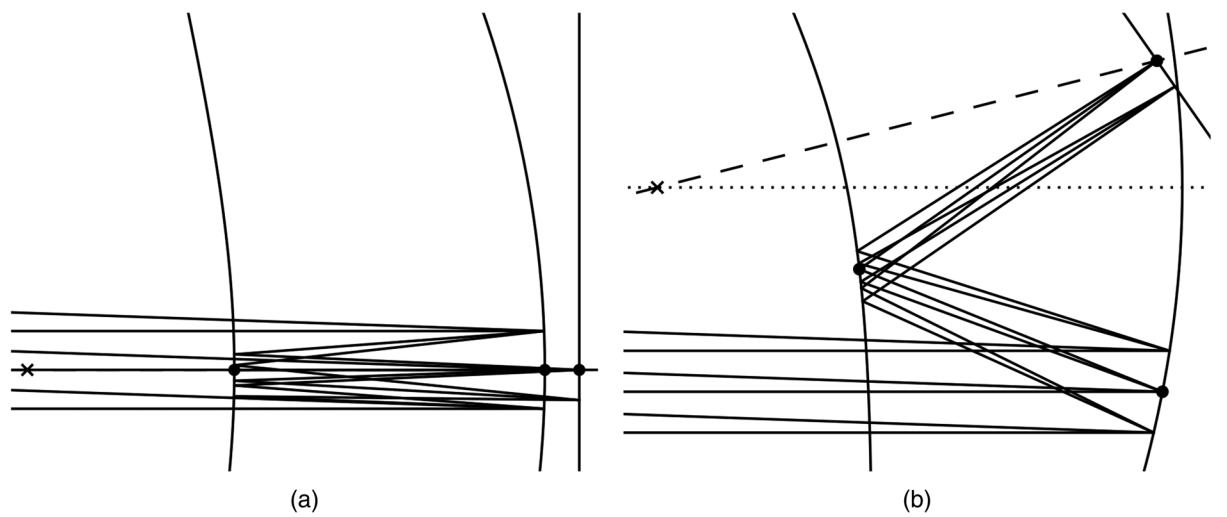

Fig. 5 Two-mirror systems: (a) a rotationally symmetric two-mirror system of confocal conics and (b) a two-mirror system of confocal conics with the primary and secondary tilted to render an unobscured system while simultaneously canceling field-asymmetric field-linear astigmatism. The dotted line is the axis of rotational symmetry for the parabolic primary, and the dashed line is the axis of rotational symmetry for the hyperbolic secondary; these axes intersect at the shared focus marked with an "X."

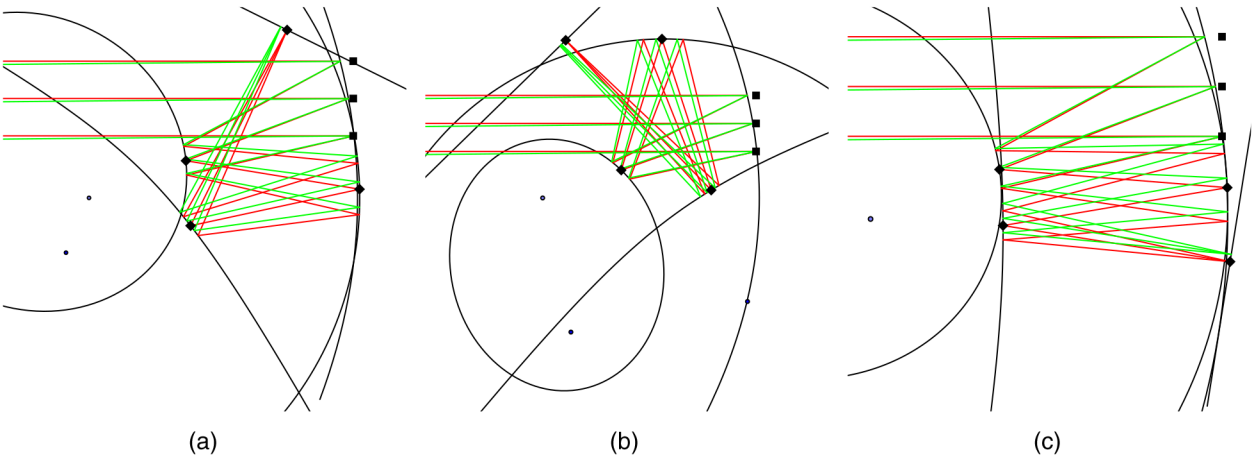

Fig. 6 Three folding geometries generated by the confocal conic layout tool for four mirror layouts (a–c), where three specific points can be repositioned to manipulate the system: the two conic foci (black circular dots, most are outside the plotted area) and the intersection point with the OAR (black diamonds). The green and red raytraces correspond to two different points in the field of view intersecting at the pupil (three black squares) and shown separated at the image plane.

through third-order if the system has a magnification with an absolute value of 1× or if the system is afocal.[9] To make a focal system with an infinite conjugate that is corrected through third-order, one cannot use only Cartesian reflectors/confocal conics; instead, aspheric deviations from the base Cartesian reflector are required. A two-mirror example of this concept is a classic rotationally symmetric Cassegrain telescope, which consists of a stigmatically imaging parabolic primary and a stigmatically imaging hyperbolic secondary, which cannot be corrected for field-linear coma. However, a two-mirror Ritchey–Chretien telescope has third-order spherical aberration introduced at the primary that is cancelled at the secondary but in such a way that the field-linear coma is also corrected.

The linear system of equations that needs to be solved to get the aspheric deviation from the Cartesian surfaces to correct for the Seidel third-order field aberrations in a four-mirror system is expressed as follows:

$$\begin{bmatrix} 1 & 1 & 1 & 1 \\ 4\left(\frac{\overline{y}_1}{y_1}\right) & 4\left(\frac{\overline{y}_2}{y_2}\right) & 4\left(\frac{\overline{y}_3}{y_3}\right) & 4\left(\frac{\overline{y}_4}{y_4}\right) \\ 4\left(\frac{\overline{y}_1}{y_1}\right)^2 & 4\left(\frac{\overline{y}_2}{y_2}\right)^2 & 4\left(\frac{\overline{y}_3}{y_3}\right)^2 & 4\left(\frac{\overline{y}_4}{y_4}\right)^2 \\ 4\left(\frac{\overline{y}_1}{y_1}\right)^3 & 4\left(\frac{\overline{y}_2}{y_2}\right)^3 & 4\left(\frac{\overline{y}_3}{y_3}\right)^3 & 4\left(\frac{\overline{y}_4}{y_4}\right)^3 \end{bmatrix} \begin{bmatrix} \Delta W_{040_1} \\ \Delta W_{040_2} \\ \Delta W_{040_3} \\ \Delta W_{040_4} \end{bmatrix} = \begin{bmatrix} \Delta W_{040} \\ \Delta W_{131} \\ \Delta W_{222} \\ \Delta W_{311} \end{bmatrix}, \tag{3}$$

where $\overline{y}_1$ is the height of the paraxial chief ray on surface 1, y_1 is the height of the paraxial marginal ray on surface 1, ΔW_{040_1} is the spherical aberration introduced by the aspheric cap on surface 1, ΔW_{040} is the total change in spherical aberration for the system, ΔW_{131} is the total change in field-linear coma for the system, ΔW_{222} is the total change in field-quadratic astigmatism for the system, and ΔW_{311} is the total change in field-cubic distortion for the system. The vector on the right-hand side is replaced with the negative of the aberration coefficients in the first-order layout made of Cartesian reflectors. The system is then solved for the vector on the left-hand side to get the amount of spherical aberration

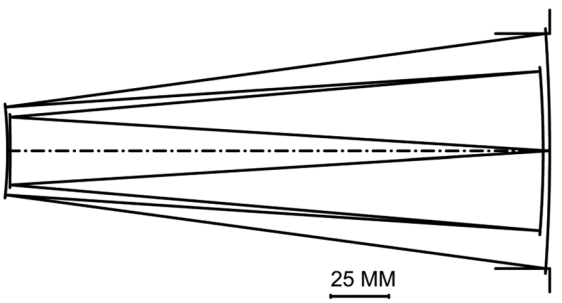

Fig. 7 Lens layout and surface descriptions for a rotationally symmetric equivalent four-mirror system to the planar-symmetric system in Fig. 6(c).

Table 2 Parameters of rotationally symmetric equivalent four-mirror system from Fig. 7.

Parameter	Mirror 1	Mirror 2	Mirror 3	Mirror 4
Radius (mm)	−743.522	−186.402	−448.0823	−1246.807
k	−1	−0.1168	−0.0161	−40.8171
A (mm^{-4})	6.4631×10^{-12}	-5.05×10^{-9}	-7.0589×10^{-10}	-6.3811×10^{-9}
Thickness (mm)	−232.8391	230.0154	−228.8836	231.3688

Table 3 Parameters describing the confocal conic system in Fig. 8. The object distance is l_o, the image distance is l_i, and the angle of incidence of the OAR is θ.

Parameter	Mirror 1	Mirror 2	Mirror 3	Mirror 4
l_o (mm)	∞	−138.922	−513.205	−168.742
l_i (mm)	−371.761	−283.19	−397.626	231.369
θ (deg)	10.482	−12.752	8.948	−9.298

Table 4 Parameters describing the confocal conic system in Fig. 9. The object distance is l_o, the image distance is l_i, and the angle of incidence of the OAR is θ.

Parameter	Mirror 1	Mirror 2	Mirror 3	Mirror 4
l_o (mm)	∞	−138.922	−513.205	−168.742
l_i (mm)	−371.761	−283.190	−397.626	231.369
θ (deg)	10.482	−12.752	8.948	−8.172

needed at each surface, and thus the amount of aspheric deviation needed at each surface.

3 Example of a Four-Mirror System

Here, we demonstrate that the aspheric caps needed for third-order aberration correction are the same for a rotationally symmetric equivalent system and the unobscured planar-symmetric system, where equivalent is defined in Sec. 3.1. To this end, we developed a tool for creating the layout of a four-mirror confocal conic system shown in Fig. 6, where the three points that needed to define a Cartesian reflector can be moved around. The three points needed are the two conic foci for stigmatic imaging, and one point on the surface, where the OAR intersects the surface. The conic foci are represented as black circular dots in Fig. 6; only the nearby conic foci are visible, the others are outside the plotted area. The intersections of the surfaces with the OAR are represented by black diamonds, as shown in Fig. 6. The entrance pupil of the system can be manipulated using the black squares in Fig. 6. This tool allows the designer to see the packaging geometry directly and manipulate the system to be unobscured and fit within a particular package shape. The designer must make the system unobscured and choose

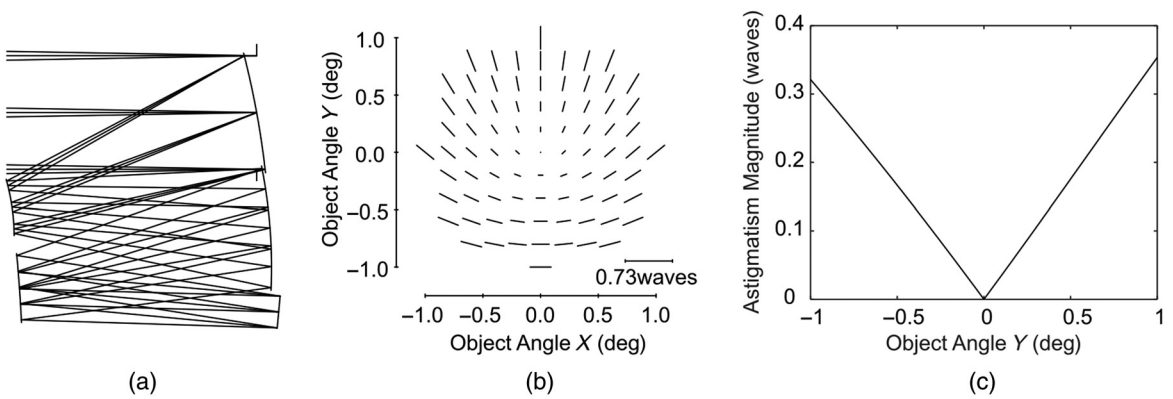

Fig. 8 Unobscured planar-symmetric confocal system: (a) lens layout; (b) full-field display of Fringe Zernike astigmatism Z5/Z6, illustrating that there is residual field-asymmetric field-linear astigmatism; (c) plot of the magnitude of the astigmatism versus the y coordinate in the field, illustrating the linear dependence of the magnitude of astigmatism with the field coordinate.

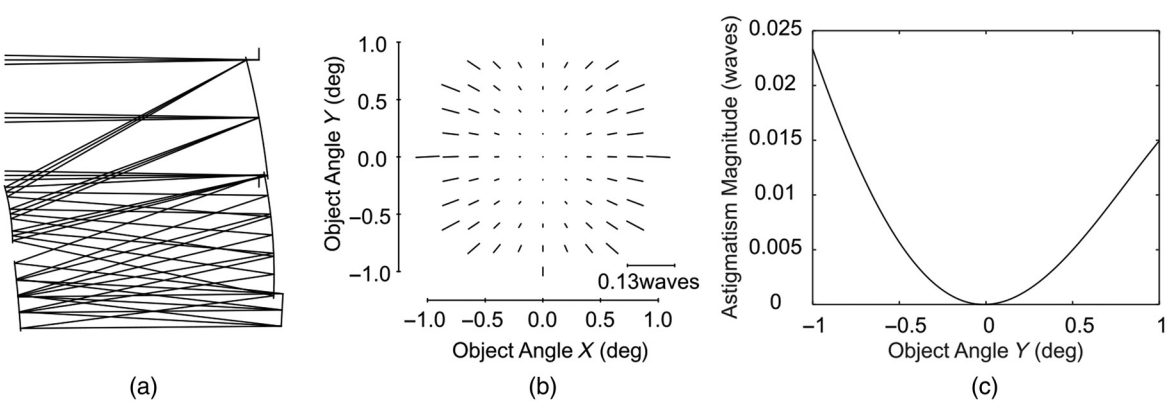

Fig. 9 Unobscured planar-symmetric confocal system with the angle of the last mirror solved to cancel field-asymmetric field-linear astigmatism: (a) lens layout; (b) full-field display of Fringe Zernike astigmatism Z5/Z6, illustrating that the residual field-asymmetric field-linear astigmatism is cancelled; (c) plot of the magnitude of the astigmatism versus the y coordinate in the field, illustrating the quadratic dependence of the magnitude of astigmatism with the field coordinate.

Table 5 Amount of spherical aberration introduced at each surface by the aspheric caps in waves at a wavelength of 587.56 nm.

	Mirror 1	Mirror 2	Mirror 3	Mirror 4
W_{040} (waves)	−0.1375	2.0949	3.1585	−0.926

the right combination of tilt angles that cancels field-asymmetric field-linear astigmatism.[15] The system in Fig. 6(c) was exported to lens design software to demonstrate the efficacy of the aberration correction.

In Sec. 3.1, we discuss a third-order aberration corrected rotationally symmetric equivalent system whose aspheric terms, which are deviations from a rotationally symmetric Cartesian reflector, are the same as the aspheric terms for a third-order system of planar-symmetric Cartesian reflectors, also known as off-axis conics with aspheric caps. In Sec. 3.2, we show the performance of the confocal conic system in Fig. 6(c) without aspheric terms added to the surface. In Sec. 3.3, we demonstrate the correction of third-order aberrations achieved by adding aspheric caps, where the coefficients of the aspheric caps are obtained from the rotationally symmetric equivalent system.

3.1 *Rotationally Symmetric Equivalent System*

Figure 7 shows a rotationally symmetric equivalent of the system in Fig. 6(c). It is equivalent in the sense that the mirror powers and separations as measured along the OAR are the same as that of the unobscured confocal conic system

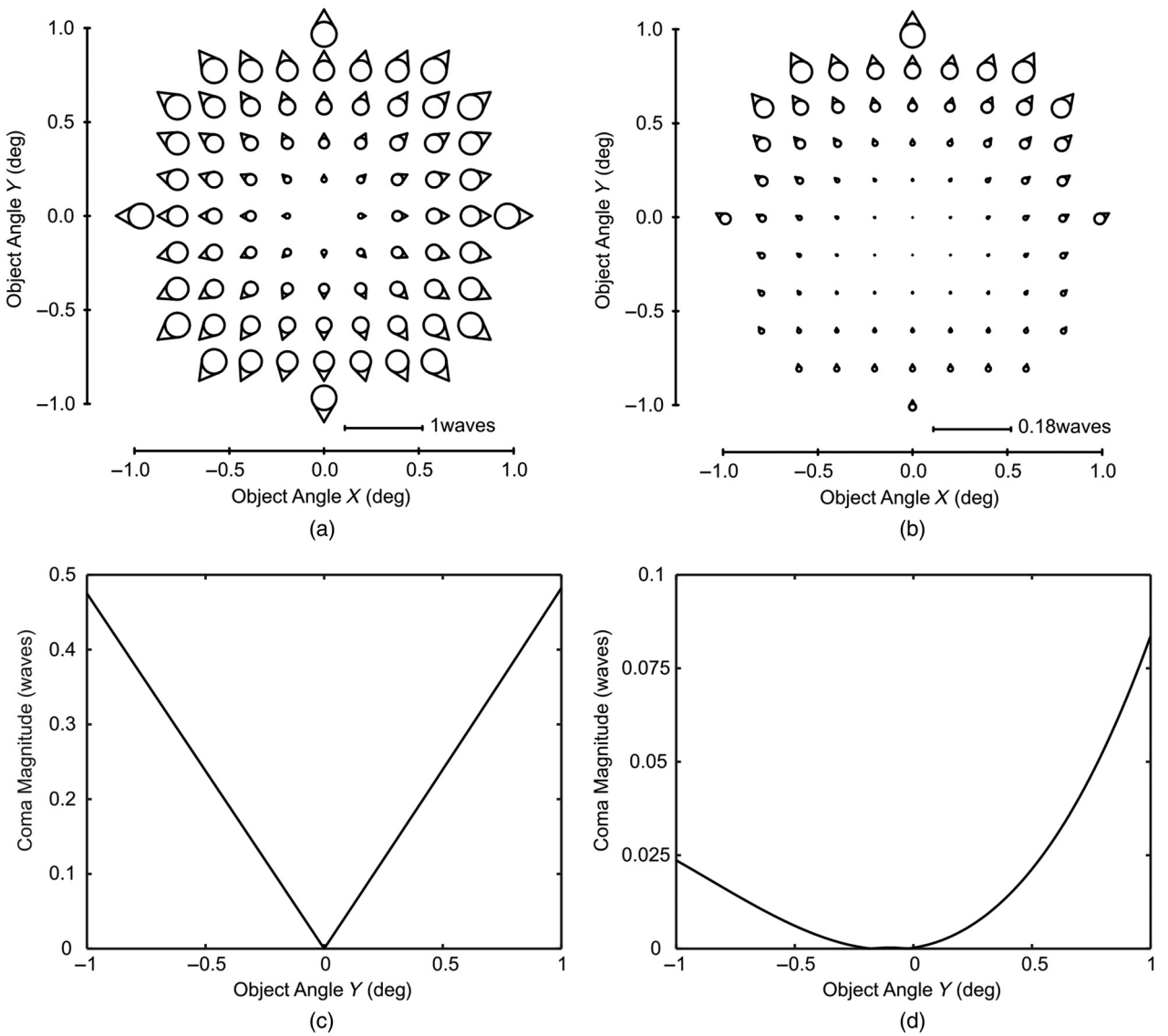

Fig. 10 Aberration plots showing that the aspheric caps were effective at eliminating field-linear coma: (a) full-field display of Fringe Zernike coma Z7/Z8 before adding the aspheric caps to the system of confocal conics; (b) same full-field display after adding the aspheric caps aberration versus the *y* field coordinate; (c) plot of the magnitude of the aberration versus the *y* field coordinate before adding the aspheric caps; and (d) plot of the magnitude after adding the aspheric caps. The worst field point before adding the aspheric caps is 0.48 waves of Z7/Z8, while the worst field point after adding the aspheric caps is 0.084 waves at a wavelength of 587.56 nm.

with the Cartesian reflector powers defined by Eq. (2) using the parameters from Eq. (1) as inputs. In Table 2, the parameters are describing the rotationally symmetric equivalent system shown in Fig. 7; the radii of curvature characterizing the mirror power for each surface as well as the conic constant k that is needed for the surface to be a Cartesian reflector with stigmatic imaging at each surface are provided. Also, the last row is the coefficient A for the fourth-order asphere that is needed to correct for the third-order field aberrations. These are the same A coefficients that are inputs to Eq. (1) that describes the shape of the freeform starting point surfaces as a base Cartesian reflector with an added aspheric cap. This system has an entrance pupil diameter of 100 mm, an effective focal length of 805 mm, and a circular field of view with a half angle of 1 deg. The system is evaluated at a wavelength of 587.56 nm for the rest of this paper. To convert this rotationally symmetric design to an unobscured planar-symmetric design, the only parameter that needs to be adjusted in Eq. (1) is the tilt angle θ, which is zero for all surfaces in a rotationally symmetric design. When θ is changed, the underlying base Cartesian reflector will change its shape but not the aspheric cap.

3.2 *Unobscured Planar-Symmetric Confocal Conic System without Aspheric Caps*

To illustrate the dominant aberration (i.e., field-asymmetric field-linear astigmatism) in a system that does not have the correct combination of tilt angles, Fig. 8(a) shows the lens layout for the unobscured planar-symmetric confocal system from Fig. 6(c); the system was exported to lens design software for evaluation. The parameters describing this system

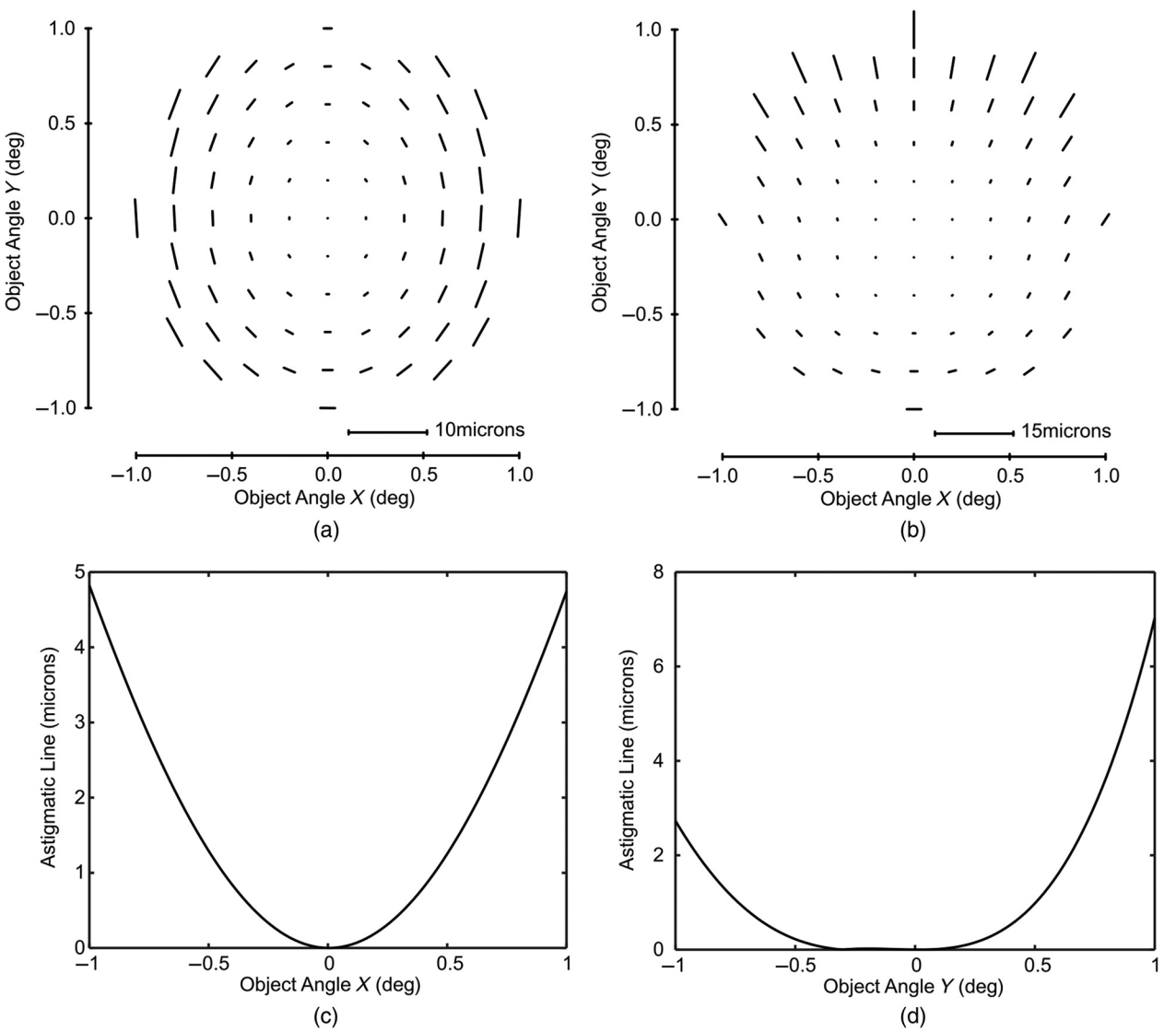

Fig. 11 Aberration plots showing that the aspheric caps were effective at eliminating field-quadratic astigmatism: (a) full-field display of the astigmatism line images as calculated by the Coddington raytrace before adding the aspheric caps to the system of confocal conics; (b) same full-field display after adding the aspheric caps; (c) associated plot of the magnitude of the aberration versus the y field coordinate before adding the aspheric caps; and (d) plot of the magnitude after adding the aspheric caps. The worst field point before adding the aspheric caps has a line of 4.8 μm, while the worst field point after adding the aspheric caps has a line of 7.0 μm.

can be found in Table 3. In this example, the tilt angle of the last mirror does not satisfy the linear astigmatism free condition, it is off by 1.12 deg, so there is residual field-asymmetric field-linear astigmatism. Figure 8(b) shows the full-field display of Fringe Zernike astigmatism Z5/Z6, illustrating the residual field-asymmetric field-linear astigmatism. The orientation of the astigmatism going halfway around the node is oriented 90 deg compared to the starting point, whereas "ordinary" rotationally symmetric astigmatism would have the same orientation going halfway around the node compared to the starting point, as shown in Fig. 4(a). Figure 8(c) is a plot of the magnitude of the astigmatism versus the y coordinate in the field, illustrating the linear dependence of the magnitude with the field coordinate.

By solving the angle of the last mirror to satisfy the linear astigmatism-free condition, the two astigmatism nodes can be brought together, making the astigmatism field closer to ordinary, as shown in Fig. 9. The parameters describing this system can be found in Table 4. The tilt was adjusted by 1.12 deg. Compared to the system in Fig. 8, cancelling the residual field-asymmetric field-linear astigmatism reduced the astigmatism of worst field point to 0.06 waves of Z5 and Z6 astigmatism compared to the 0.35 waves. The orientation of the astigmatism is now the same going halfway around the node compared to the starting point, and the field dependence of the magnitude is quadratic.

3.3 *Unobscured Planar-Symmetric Confocal Conic System with Aspheric Caps*

Once the aberrations are "ordinary" again, the aspheric caps from Sec. 3.1 can be put on top of the Cartesian reflector base surfaces. These aspheric caps will correct for the rest of the third-order aberrations. The amount of spherical aberration introduced at each surface by the aspheric caps, as determined by Eq. (3), is shown in Table 5.

Figure 10 shows the full-field displays of Z7 and Z8 Fringe Zernike coma before and after adding the aspheric caps. Before adding the caps, the field dependence of the magnitude of the coma was linear. After adding the caps, the field dependence of the magnitude of the coma is quadratic and the worst field point was reduced from 0.48 waves to 0.084 waves of coma. This shows that the aspheric caps were effective at canceling the field-linear coma as expected.

Figure 11 shows full-field displays of the astigmatism line images as calculated by the Coddington raytrace in CODE V. In this computation, the Coddington raytrace option is shown instead of the Fringe Zernike pupil fit because there is a nonzero contribution from higher order aberrations after adding the aspheric caps, which makes it appear as if there is a field constant dependence of astigmatism. The worst field point before adding the aspheric caps has a 4.8 μm line, while the worst field point after adding the aspheric caps has a line of 7.0 μm. The field dependence of the magnitude around the center of the field went from quadratic before adding the aspheric caps to quartic after adding the aspheric caps, demonstrating the efficacy of the aspheric caps at eliminating the field-quadratic astigmatism.

Figure 12 shows full-field displays of Z9 Fringe Zernike spherical aberration before adding the aspheric caps and after. The goal of adding the caps is to correct for the field aberrations without introducing a large amount of spherical aberration. The worst field point after adding the caps has 0.015 waves of spherical aberration, even though a few waves of spherical aberration are introduced at the individual surfaces; the total spherical aberration after summing the individual surface contributions is small.

Figure 13 shows full-field displays of the RMS wavefront error before and after adding the aspheric caps. The aspheric caps reduced the worst field point from an RMS wavefront error of 0.17 waves to 0.09 waves, demonstrating the efficacy of the aspheric caps at improving performance of design.

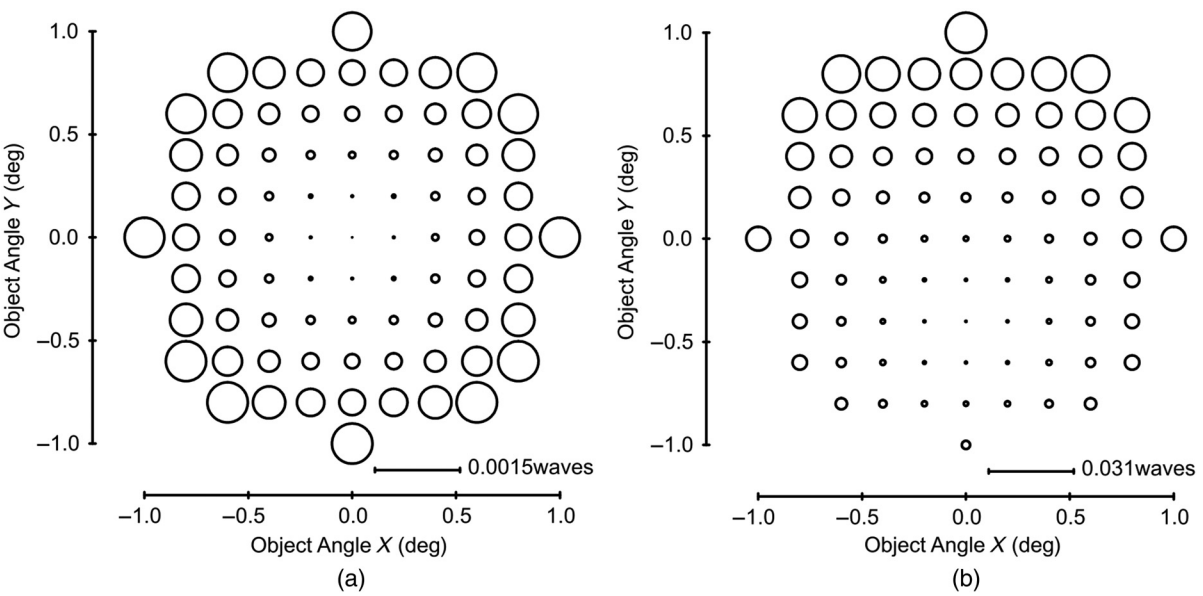

Fig. 12 Aberration plots showing that the aspheric caps did not add large amounts of spherical aberration: (a) full-field display of Fringe Zernike spherical aberration Z9 before adding the aspheric caps to the system of confocal conics; (b) same full-field display after adding the aspheric caps. The worst field point before adding the aspheric caps is 0.00071 waves of Z9, while the worst field point after adding the aspheric caps is 0.015 waves at a wavelength of 587.56 nm. The aspheric caps did not introduce a large amount of spherical aberration.

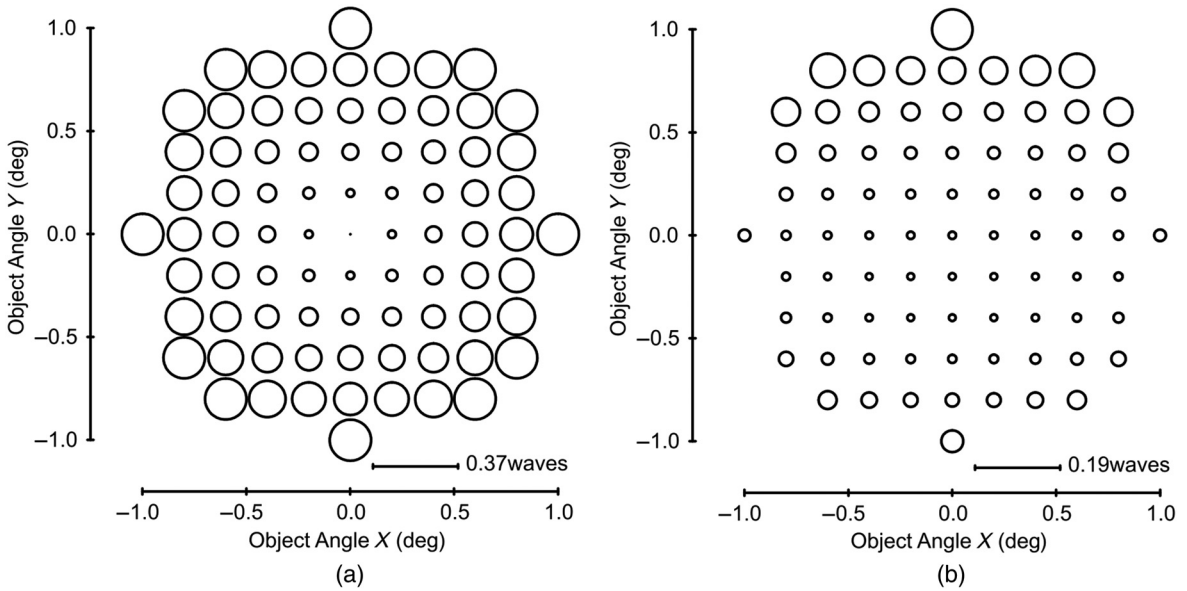

Fig. 13 RMS wavefront error full-field display plots: (a) before adding the aspheric caps and (b) after adding the aspheric caps. The worst field point before adding the aspheric caps is 0.17 waves of RMS wavefront error, while the worst field point after adding the aspheric caps is 0.090 waves of RMS wavefront error at a wavelength of 587.56 nm.

4 Conclusion

Several analytical starting point design methods have been considered with various symmetries and states of correction. It is shown in this paper that a combination of these methods allows for unobscured starting points that are corrected for the third-order image degrading aberrations. The tool and procedures outlined in this paper were applied to generate four-mirror starting points for freeform designs, whose surfaces are base Cartesian reflectors with aspheric caps to correct the field aberrations. These starting points are limited by higher order aberrations that can then be corrected by adding and optimizing freeform terms for the surfaces.

Appendix: Sag of Cartesian Reflectors in their Local Coordinate Systems

The equation for the sag of a Cartesian reflector in the local coordinate system of the surface is first given and then derived. Let the object and image vergences be the reciprocal of the object and image distances (i.e., $V_o = 1/l_o$ and $V_i = 1/l_i$) such that an object or image at infinity will result in a vergence of zero. The angle θ is the angle of incidence of the OAR, and x and y are the local coordinates. The sag of a Cartesian reflector in terms of these variables, denoted as $\mathrm{Sag}_{\text{Cartesian Reflector}}(V_o, V_i, \theta, x, y)$, may then be expressed as follows:

$$\mathrm{Sag}_{\text{Cartesian Reflector}}(V_o, V_i, \theta, x, y) = \frac{(A+B)}{C}, \tag{4}$$

$$A = 2(V_i + V_o)\cos(\theta)[2 + (V_o - V_i)y\,\sin(\theta)], \tag{5}$$

$$B = -(V_i+V_o)\sqrt{2}\sqrt{[4-(V_i^2+6V_iV_o+V_o^2)x^2-4V_oV_iy^2+(4+(V_i-V_o)^2x^2-4V_iV_oy^2)\cos(2\theta)+8(V_o-V_i)y\cos^2(\theta)\sin\theta]}, \tag{6}$$

$$C = [V_i^2 + 6V_iV_o + V_o^2 - (V_i - V_o)^2\cos(2\theta)]. \tag{7}$$

This is an exact equation for the sag of a Cartesian reflector in the local coordinate system, where the OAR is incident with the origin, the slope of the surface is zero at the origin, and the sag of the surface at the origin is zero (i.e., the $x-y$ plane of the local coordinate system is tangent to the surface at the origin). Using the coordinate system in Fig. 1, the location of the stigmatic imaging points can be conveniently written in terms of l_o, l_i, and θ. The Cartesian reflector is then solved by writing that the geometrical path for all points on the surface is constant and equal to the sum of the vergences V_o and V_i, a property of conic sections of revolution, which is given as follows:

$$\frac{1}{V_o}+\frac{1}{V_i} = \sqrt{x^2+\left[y+\frac{1}{V_o}\sin(\theta)\right]^2+\left[z-\frac{1}{V_o}\cos(\theta)\right]^2} + \sqrt{x^2+\left[y-\frac{1}{V_i}\sin(\theta)\right]^2+\left[z-\frac{1}{V_i}\cos(\theta)\right]^2}, \tag{8}$$

where x, y, and z are the coordinates of points on the surface of the Cartesian reflector. To get Eq. (4), solve Eq. (8) for z as a function of x, y, V_o, V_i, and θ, which will give the sag in the local coordinate system.

Disclosures

We report grants from NASA (NNX16AM90H) during the conduct of the study.

Acknowledgments

We acknowledge a NASA Space Technology Research Fellowship to Jonathan Papa (NNX16AM90H) that supports this research. We thank Synopsys Inc. for the student license of CODE V. This research synergizes with the NSF I/UCRC Center for freeform optics (IIP-1338877, IIP-1338898). A part of this work was previously reported in a conference proceeding.[17]

References

1. J. M. Howard and B. D. Stone, "Imaging with four spherical mirrors," *Appl. Opt.* **39**, 3232–3242 (2000).
2. K. Fuerschbach, J. P. Rolland, and K. P. Thompson, "A new family of optical systems employing φ- polynomial surfaces," *Opt. Express* **19**(22), 21919–21928 (2011).
3. K. Fuerschbach, J. P. Rolland, and K. P. Thompson, "Interferometric measurement of a concave, φ-polynomial, Zernike mirror," *Opt. Lett.* **39**(1), 18–21 (2014).
4. P. Benitez, M. Nikolic, and J. C. Miñano, "Analytical solution of an afocal two freeform mirror design problem," *Opt. Express* **25**(4), 4155–4161 (2017).
5. T. T. Elazhary et al., "Optical design method for freeform optics," in *Renewable Energy and the Environment*, Optical Society of America, OSA Technical Digest, paper FM4B.4 (2013).
6. K. P. Thompson et al., "A real ray-based method for locating individual surface aberration field centers in imaging optical systems without symmetry," *J. Opt. Soc. Am. A* **26**(6), 1503–1518 (2009).
7. H. A. Buchdahl, *An Introduction to Hamiltonian Optics*, Dover, New York (1993).
8. J. M. Sasian, "How to approach the design of a bilateral symmetric optical system," *Opt. Eng.* **33**(6), 2045–2061 (1994).
9. D. Korsch, *Reflective Optics*, pp. 224–225, Academic Press, Boston, Massachusetts (1991).
10. A. Rakich, "Four-mirror anastigmats, part 1: a complete solution set for all-spherical telescopic systems," *Opt. Eng.* **46**(10), 103001 (2007).
11. K. Fuerschbach, J. P. Rolland, and K. P. Thompson, "Theory of aberration fields for general optical systems with freeform surfaces," *Opt. Express* **22**(22), 26585–26606 (2014).
12. A. Bauer, E. M. Schiesser, and J. P. Rolland, "Starting geometry creation and design method for freeform optics," *Nat. Commun.* **9**, 1756 (2018).
13. J. R. Rogers, "Vector aberration theory and the design of off-axis systems," *Proc. SPIE* **0554**, 76–81 (1985).
14. K. Thompson, "Description of the third-order optical aberrations of near-circular pupil optical systems without symmetry," *J. Opt. Soc. Am. A* **22**(7), 1389–1401 (2005).
15. S. Chang, "Linear astigmatism of confocal off-axis reflective imaging systems with N-conic mirrors and its elimination," *J. Opt. Soc. Am. A* **32**, 852–859 (2015).
16. D. Korsch, "Closed-form solutions for imaging systems, corrected for third-order aberrations," *J. Opt. Soc. Am. A* **63**(6), 667–672 (1973).
17. J. C. Papa, J. M. Howard, and J. P. Rolland, "Starting point designs for freeform four-mirror systems," *Proc. SPIE* **10590**, 105900Z (2017).

Jonathan C. Papa is a PhD student in optics at the University of Rochester. He received his BS degree in physics and a BS degree in optical engineering from the University of Rochester in 2014. His current research focuses on the design of multiple mirror freeform reflective imaging systems.

Joseph M. Howard received BS degree in physics from the US Naval Academy in Annapolis, Maryland, and his PhD in optical design from The Institute of Optics, University of Rochester, in Rochester, New York. He now serves as the lead optical designer for NASA on the James Webb Space Telescope Project, which is the successor to Hubble Space Telescope.

Jannick P. Rolland is the Brian J. Thompson professor of optical engineering at the Institute of Optics at the University of Rochester, in Rochester, New York, where she directs the NSF I/UCRC Center for Freeform Optics (CeFO), the R.E. Hopkins Center for Optical Design and Engineering, and the ODALab. She earned an optical engineering diploma from the Institut D' Optique, France, and a PhD in optical sciences from the College of Optical Sciences at the University of Arizona.